JOURNAL OF MATERIALS SCIENCE 5 (1970) 992–1004

Solidification of Aluminium-Germanium Alloys at High Cooling Rates

C. SURYANARAYANA, T. R. ANANTHARAMAN
Department of Metallurgy, Banaras Hindu University, Varanasi-5, India

Aluminium-germanium alloys, covering the entire composition range, were subjected to rapid solidification by different techniques ranging from the gun technique of splat cooling to simple quenching of the melt in water. The constitution, microstructure and crystal structure of the alloys thus solidified under cooling rates varying from 10^3 to 10^7° C/sec were studied by standard optical, electron- and X-ray metallographic techniques.

The solid solubility of Ge in Al could be increased from the equilibrium value of 2.8 at. % to a maximum of 7.2 at. %. In addition, two new non-equilibrium tetragonal phases γ_1(a = 12.91 to 13.11 Å, c = 12.00 to 12.10 Å) and γ_2(a = 14.98 Å, c = 16.03 Å) could be obtained in alloys containing 15 to 40 and 40 to 80 at. % Ge respectively. In relation to the face-centred cubic α solid solution, these appear to be made up of 30 and 52 unit cells, respectively, with the relations $a_{\gamma_1} \simeq \sqrt{10}a_\alpha$, $c_{\gamma_1} \simeq 3a_\alpha$ and $a_{\gamma_2} \simeq \sqrt{13}a_\alpha$, $c_{\gamma_2} \simeq 4a_\alpha$.

A new non-equilibrium constitution diagram connecting cooling rate with constitution at room temperature has been proposed and seems to explain all observations satisfactorily.

1. Introduction

There has been considerable interest in the last decade in studying the impact of high quenching rates on the solidification behaviour of alloys. The most spectacular among the new liquisol*-quenching techniques is the "gun" technique developed by Duwez and his collaborators [1] and popularly referred to as the *splat-cooling* or *splat-quenching* technique. Here, a small molten droplet of a material is allowed to solidify at very high cooling rates, of the order of 10^6 to 10^8 ° C/sec [2, 3], by rapid spreading of a thin foil on a heat-conducting substrate. The application of this quenching technique has led to the formation of a large number of non-equilibrium intermediate phases, in addition to striking extensions of solid solubility limits as well as amorphous solidification, in various binary and ternary alloy systems. Many of the missing Hume-Rothery phases in noble metal systems, such as the 7:4 electron compounds in Ag-Ge [4], Au—Ge [5] and Ag—Si [6] systems and the 21:13 electron compounds in Au—Si [7] and Au—Sn [8] systems, have been prepared with the help of this rapid quenching technique. All such new phases seem to be metastable, in that they decompose when aged at room temperature or annealed at higher temperatures well below the solidus. Such non-equilibrium phenomena have been observed over a very wide range of temperatures, varying from as low as 170° K [9] to as high as 870° K [10], depending upon the system under consideration. A large number of reviews embodying the results so far obtained is now available in literature [11-14].

The impact of a range of cooling rates on solidification has so far not been studied systematically in any system, although the dependence of constitution on the thickness of the solidified foil has been clearly noted in many investigations [15, 16]. We present here the results of a fairly comprehensive study of the influence of cooling rates in the range of 10^3 to 10^7 ° C/sec on the solidification of aluminium-germanium alloys.

The aluminium-germanium phase diagram features a simple eutectic at 30.3 at. % Ge and 424° C, with a maximum solid solubility of 2.8

*As the expression *quenching* has come to be associated with the solid state, particularly in the metallurgical world, it is considered necessary to evolve other expressions to refer to rapid cooling techniques involving the liquid and gaseous states. *Liquisol-quenching* and *Vaposol-quenching* are suggested for rapid cooling involving transition from liquid to solid and vapour to solid, respectively. *Liquid-quenching* and *Vapour-quenching* may then connote rapid cooling of liquids and gases from a high to a low temperature.

at. % Ge in Al at the eutectic temperature and of 0.97 at. % Al in Ge at 575° C [17]. The solid solubility of Ge in Al at room temperature is practically negligible (fig. 1). Predecki *et al* [7] have reported the formation of a complex non-equilibrium phase in an Al-30 at. % Ge alloy.

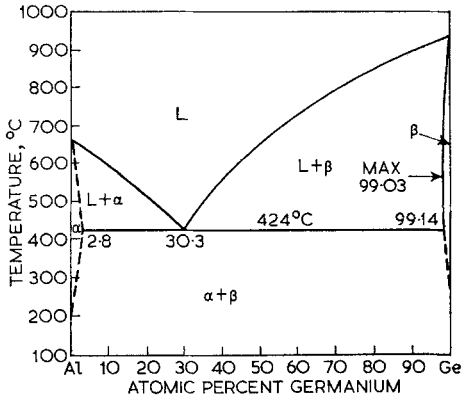

Figure 1 Aluminium-germanium equilibrium diagram.

The structure of this phase has since been established by us [18] as tetragonal with $a = 13.03$ Å and $c = 12.04$ Å. Predecki *et al* [7] have also reported an extension of the solid solubility limit on the aluminium side of the diagram, but without any quantitative indication. Another non-equilibrium phase has recently been detected by us [19] in an Al-50 at. % Ge alloy quenched from the melt. In the present study alloys covering the whole binary system have been systematically subjected to different rates of solidification and examined in the metallurgical microscope as well as the electron microscope and also by X-ray methods.

2. Experimental Procedure

2.1. Preparation of Alloys

Fifteen alloys were prepared from aluminium of 99.99 + % and germanium of 99.9999 + % purity. Required quantities of the two metals were weighed out for a 3g charge and melted in an evacuated fused silica capsule. After the alloys were molten, the melt was thoroughly agitated to effect homogenisation and then the capsules were chilled in water. The alloys were then cold-worked, wherever possible, and homogenised at 300° C *in vacuo* for a period of 120 h. From the difference in weight of the alloy before and after melting, it could be concluded that the compositions indicated are accurate at least to ± 1.0 at. %.

2.2 Liquisol-Quenching Techniques

The apparatus used for liquisol-quenching in the present investigation is similar to the one developed by Duwez and Willens [1] and has been described in detail elsewhere [20]. A graphite crucible with a replaceable insert which has a very fine nozzle (1.5 mm diameter and 25 mm long) at the bottom, is heated to the desired temperature in a resistance-heated furnace. After the required temperature is reached, a small quantity (20 to 50 mg) of the material is charged into the crucible. It melts, but stays in position above the orifice because of surface tension. This whole assembly is then swung into position so that the opening of the crucible is in the path of the shock wave.

The shock wave is generated by the rupture of a mylar diaphragm (about 0.05 mm thick) separating the high-pressure chamber and the low-pressure chamber, as shown in fig. 2. An inert gas, such as argon, enters the high-pressure chamber until the pressure is enough to rupture the mylar diaphragm. The resulting shock wave propagates without any appreciable loss of intensity at a high speed of about 300 m/sec and forcibly ejects the molten droplet through the orifice. The liquid droplet then spreads on the substrate and cools rapidly to room temperature. Since the cooling rate is directly dependent upon the efficiency of heat removal from the liquid droplet, the material of the substrate becomes very important. Generally, a good heat conductor such as copper is used.

In an effort to vary the cooling rate, the copper substrate was substituted at times in our work by a beaker of water at room temperature. In further variations of this technique, the melt was just dropped either onto a copper substrate or into water without the help of any shock wave. The cooling rate naturally decreased in the order mentioned and could be roughly estimated in each case, as described later (section 2.3).

The products of rapid solidification were either thin foils of varying cross-section when the substrate used was copper, or fine powder when the quenching was in water. Some of the foils in the former case were thin enough for direct examination in a Philips EM 200 electron microscope at 60 kV. However, in case of experiments where the melt was merely dropped onto a copper substrate, it was, in most cases,

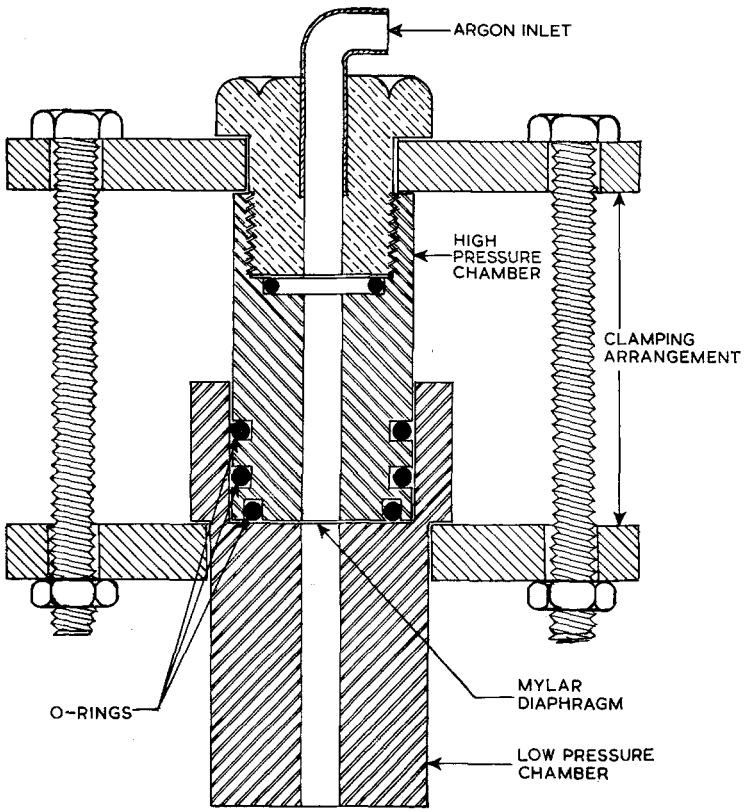

Figure 2 Section of the shock tube in the apparatus for liquisol-quenching.

difficult to get thin enough flakes suitable for X-ray "powder" specimens. Invariably the melt solidified in rather thick flakes. Therefore, this type of cooling was attempted only on two or three representative alloys covering either side of the eutectic composition. Further discussions will therefore be confined mainly to the results obtained from the other three quenching techniques.

2.3. Estimation of Quenching Rates

Although many attempts – theoretical and experimental – have been made to estimate the high cooling rates developed in liquisol-quenching techniques, the methods developed are either very approximate or time-consuming. They include theoretical calculations, as developed by Ruhl [3], measurement of emf generated when the splat covers two dissimilar metals, as attempted by Predecki *et al* [2], and study of the intensity of infra-red radiation emanated by the splat, as tried by Löhberg and Müller [21]. Even when reliable estimates of cooling rates could be obtained employing any of the above methods, these do not take into consideration any of the structural characteristics of the splat. An improved method has been developed by Matyja *et al* [22], wherein a correlation is arrived at between dendrite arm spacing (DAS) and the cooling rate. This method is simple as well as straightforward and is based on the fact that DAS is a function of supercooling, which in turn depends on the rate of quenching. Matyja *et al* [22] have given a master diagram correlating secondary DAS in Al-base alloys with cooling rates over ten orders of magnitude. Hence, if DAS could be measured accurately, the rate at which the splat solidified could be estimated directly from this master diagram.

The method developed by Levy *et al* [23] was employed in the present study to calculate DAS. It is highly selective in that the surface of the splat foil must run parallel to and through a primary arm. A sectioning (scan) line is then drawn parallel to a primary arm such that it intersects the maximum number of secondary arms. The number of secondary arms in that segment is then counted and the calculation follows from the relation:

$$d = L \times 10^4/(n-1)M \qquad (1)$$

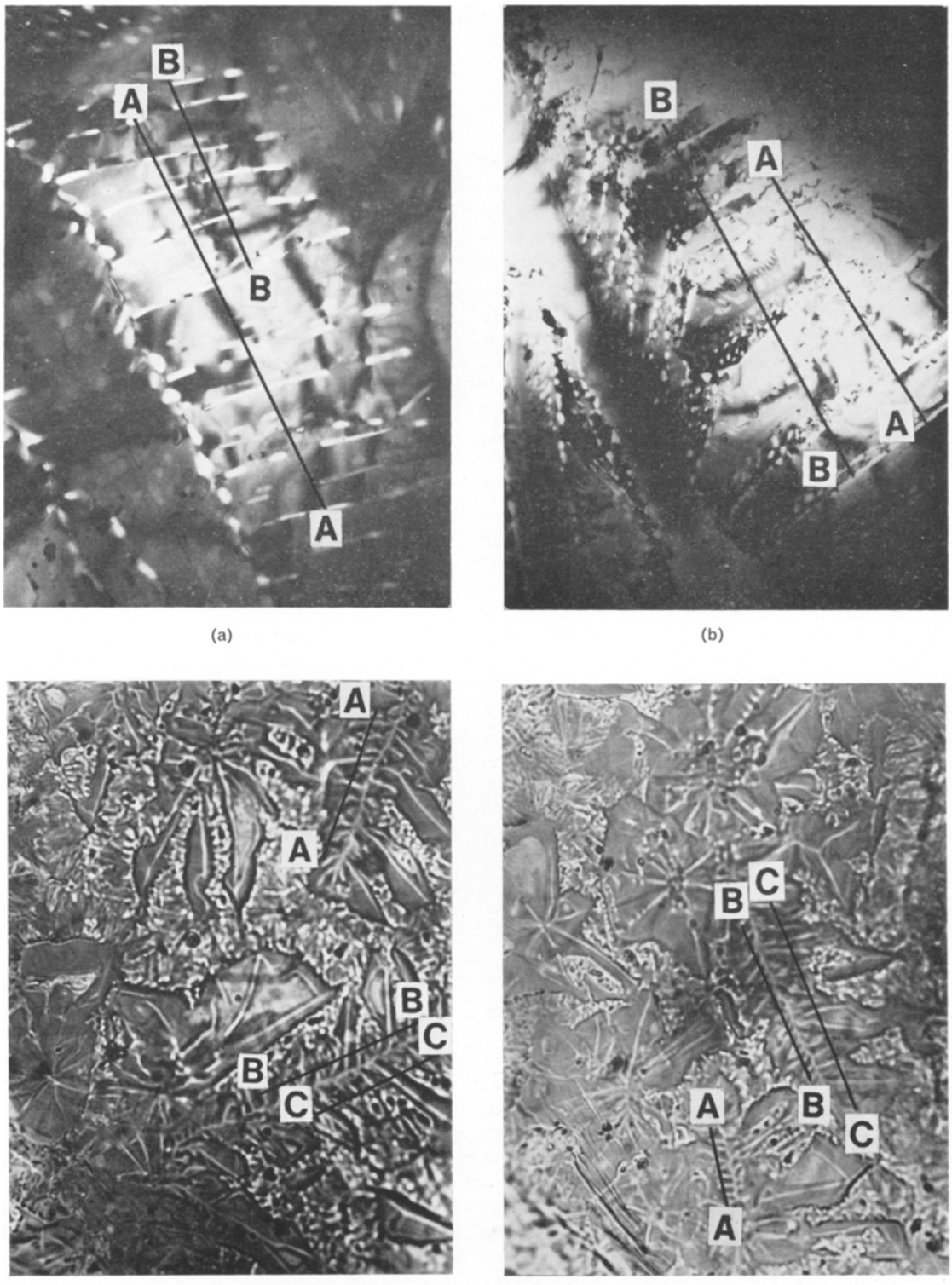

Figure 3 Photomicrographs used for measurement of secondary dendrite arm spacing. (a) and (b) electron micrographs of foils of Al-40 at.% Ge alloy quenched by the "gun" technique (× 12900). (c) and (d) optical micrographs of Al-45 at.% Ge alloy solidified by dropping the melt onto a copper substrate (× 1000).

where d = secondary DAS (in microns), L = length of scan line (in cm), n = number of intersections of scan line with high solute regions (convention is to begin and end the scan line on a high solute region), and M = magnification of the photomicrograph.

The values of DAS obtained by this method are shown in table I. The scan lines are drawn on the photomicrographs in figs. 3a to d. Figs. 3a and b are electron micrographs of splat foils obtained by the "gun" technique and figs. 3c and d are optical micrographs of foils obtained when the melt was dropped onto a copper substrate without the help of a shock wave. A great advantage with these foils is that they do not require any metallographic preparation and all structural features are visible in the as-quenched condition itself. Since microstructures could not be observed in the other two cases when the melt was (i) shot or (ii) dropped into water (and thereby turned into powder), the cooling rates were qualitatively estimated to be between the above-mentioned cooling rates for (i) and lowest of all for (ii).

Since the cooling rate varies as a function of thickness, there are bound to be effectively different cooling rates in different regions of the foils obtained by the "gun" technique. Although the cooling rates were of a constant order of magnitude for a particular technique, it is important to remember that the cooling rates estimated with the help of electron micrographs could be on the higher side since only very thin foils, transparent to the electron beam, were thus examined. On the other hand, in the other techniques, the cooling rate could be slightly lower, since relatively thicker flakes were observed in the optical microscope.

2.4. X-ray Examination

In experiments where the heat was abstracted by a copper substrate, the resulting foils did not stick to the substrate and could be easily removed by gentle tapping and without introducing any plastic deformation. Fine flakes were collected and mounted around a thin glass fibre with the help of "Quickfix" to make a suitable specimen for X-ray examination. In cases, where the melt was either shot or dropped into water, the fine powder was separated from water by filtration, thoroughly washed with alcohol and then dried. This fine powder was then used to prepare a specimen, as before, for X-ray examination. The Debye-Scherrer patterns were obtained in a Philips 114.6 mm diameter camera with nickel-filtered Cu Kα radiation. Typical exposure conditions were 36 kV, 16 mA and 4 h.

Film shrinkage correction was applied and the interplanar spacings recorded were generally the mean of at least three or four measurements. The lattice parameters of α-solid solution were calculated with the maximum possible accuracy ($\pm$ 0.001 Å) by extrapolation against the Nelson-Riley function.

3. Results

3.1. New Phases and their Crystal Structures

Most X-ray powder patterns consisted of a large number of extra reflections in addition to the reflections due to equilibrium α and/or β solid solutions. The complex of reflections from different phases naturally depended on the composition of the alloy and the cooling rate employed, but all X-ray patterns could be indexed in terms of one or more of four different phases, namely the α and β terminal solid solutions and two new non-equilibrium tetragonal phases, designated γ_1 and γ_2. The results are collected in tables I to IV.

The number and proportion of the phases was greatly influenced by the nature of the liquisol-quenching technique adopted. To refer to the results with the "gun" technique, for example, in alloys between 15 and 40 at. % Ge both α and γ_1 seem to exist together, whereas between 40 and 80 at. % Ge, β and γ_2 appear to be the phases present. However, around 40 at. % Ge both γ_1 and γ_2 are found to coexist. However, the temperature from which the melt is quenched does not seem to have any effect on the constitution of the alloys at room temperature, unlike some previous observations [14].

A somewhat unexpected result of the present investigation was the formation of the new phases γ_1 and γ_2, even when the melt was just dropped either onto a conducting substrate such as copper, or into water. Although the cooling rate in these two techniques is considerably lower than in the other two, no qualitative change in the constitution was observed in comparison with the products of the faster quenching techniques (see table IV). However, with decreasing cooling rate the fractional amount of the terminal solid solutions of a given alloy went on increasing. For example, α phase could not be detected when alloys containing more than 40 at. % Ge were subjected to liquisol-quenching by the "gun" technique. But the amount of α phase

TABLE I Estimation of cooling rate from secondary dendrite arm spacing (DAS).

Figure	Scan line	L(cm)	$(n-1)$	M	$d(\mu)$	$d_{av}(\mu)$	Average cooling rate, °C/sec
3a	AA	6.5	9	12 900	0.56	0.53	$\sim 2 \times 10^6$
	BB	3.2	5	12 900	0.50		
3b	AA	4.4	6	12 900	0.57	0.53_5	$\sim 2 \times 10^6$
	BB	6.4	10	12 900	0.50		
3c	AA	2.45	13	1000	1.88		
	BB	2.95	17	1000	1.74	1.95	$\sim 4 \times 10^4$
	CC	2.45	11	1000	2.23		
3d	AA	1.25	8	1000	1.56		
	BB	2.8	14	1000	2.00	1.92	$\sim 4 \times 10^4$
	CC	3.5	16	1000	2.19		

increased significantly with a decrease in the cooling rate. Thus, both α and β phases become quite prominent, in addition to γ_2, in alloys containing 40 and 50 at. % Ge. Obviously, the critical cooling rate for the formation of the non-equilibrium Al-Ge phases is not very high. This seems to be the first case where new non-equilibrium structures have been produced at comparatively low cooling rates and been found to be quite stable at room temperature, as will be discussed later (section 4.5).

The lattice parameter of α solid solution was found to reach a maximum value of 4.0615 Å. This corresponds to an extension of solid solubility of Ge in Al to 7.2 at. % according to available data [24] on the variation of the lattice parameter of Al-solid solution with Ge content, which can be expressed by the relation:

$$a_\alpha = 4.0495 + 0.00166\, C_{Ge}\text{Å}$$

where C_{Ge} is the concentration of germanium in at. %. However, there was no lattice parameter evidence for any extension of solid solubility of Al in Ge.

The Debye-Scherrer patterns of alloys containing 15 to 40 at. % Ge consisted of a large number of extra reflections, mostly diffuse and sharp in only a few cases. All the extra reflections in these patterns conld be satisfactorily indexed on the basis of a tetragonal structure (γ_1) with a possible 120 atoms per unit cell and with the lattice parameters $a_{\gamma_1} \simeq \sqrt{10}a_\alpha$ and $c_{\gamma_1} \simeq 3a_\alpha$, where a_α is the lattice parameter of the hypothetical α solid solution having the same germanium content as the γ_1 phase. Table II brings out the regular variation in intensity and interplanar spacings of the various reflections at different concentrations of germanium. From the observed variation between 15 and 40 at. % Ge, it can be concluded that the lattice parameters of γ_1 vary according to the following relations:

$$a_{\gamma_1} = 12.91 + 0.008\, C_{Ge}\text{Å}$$

and

$$c_{\gamma_1} = 12.10 - 0.004\, C_{Ge}\text{Å}\,.$$

Between 40 and 80 at. % Ge another set of reflections, which was sharper than in the previous case, was observed with interplanar spacings quite different from those observed at lower germanium contents. All the reflections in alloys containing between 40 and 80 at. % Ge could be satisfactorily indexed on the basis of another tetragonal structure (γ_2) with no less than 208 atoms per unit cell and with the lattice parameters $a_{\gamma_2} = 14.98$ Å and $c_{\gamma_2} = 16.03$ Å. The lattice parameters of the γ_2 tetragonal structure are related to the α solid solution by the relation $a_{\gamma_2} \simeq \sqrt{13}a_\alpha$ and $c_{\gamma_2} \simeq 4a_\alpha$, where a_α is the lattice parameter of the hypothetical α solid solution containing 50 at. % germanium. Table III brings out the good agreement between the observed and calculated interplanar spacings for an Al-50 at. % Ge alloy. No significant variation of the interplanar spacings with germanium content was observed for the γ_2 structure.

3.2. Stability of the Non-equilibrium Phases

Cold working of the samples at room temperature did not transform the new phases, but only broadened the X-ray reflections further. All the extra lines in the Debye-Scherrer patterns continued intact even after ten months at room temperature. However, the new phases showed signs of decomposition after heating to 200° C and disappeared completely when held at 300° C for about 30 min. The decomposition of the new phases is studied by taking powder

TABLE II Observed and calculated lattice spacings of γ_1 non-equilibrium phase in the Al—Ge System Range of composition: $Al_{80}Ge_{20}$—$Al_{60}Ge_{40}$ Structure: Tetragonal, lattice parameters: $a\gamma_1 \simeq \sqrt{10}a_\alpha$; $c\gamma_1 \simeq 3a_\alpha$; $c/a = 3/\sqrt{10}$

Lattice parameter	$a = 12.95$Å; $c/a = 0.932_6$ (Al-20 at. % Ge)			$a = 12.99$Å; $c/a = 0.928_1$ (Al-25 at. % Ge)			$a = 13.03$Å; $c/a = 0.923_8$ (Al-30 at. % Ge)			$a = 13.06$Å; $c/a = 0.921_2$ (Al-33.3 at. % Ge)			$a = 13.11$Å; $c/a = 0.915_4$ (Al-40 at. % Ge)		
hkl	d_{cal}(Å)	d_{obs}(Å)	I_{obs}	d_{cal}(Å)	d_{obs}(Å)	I_{obs}	d_{cal}(Å)	d_{obs}(Å)	I_{obs}	d_{cal}(Å)	d_{obs}(Å)	I_{obs}	d_{cal}(Å)	d_{obs}(Å)	I_{obs}
030	4.316	4.316	vvw	4.329	4.323	vw	4.341	4.331	vw	—	—	—	4.370	4.319	vw
230	3.589	3.562	vvw	3.604	3.587	w	3.614	3.606	vw	3.621	3.607	vw	—	—	—
023	3.417	3.414	w	3.417	3.391	vvw	3.417	3.386	vvw	3.417	3.417	ms	3.414	3.404	vvw
123	—	—	—	3.306	3.321	w	—	—	—	3.306	3.306	s	3.306	3.317	vw
040	3.238	3.224	vw	3.248	3.230	vw	3.258	3.269	vw	3.263	3.255	vvw	—	—	—
223	3.021	3.021	vvw	—	—	—	3.026	3.024	w	3.026	3.019	vw	—	—	—
133	2.878	2.883	vvw	2.873	2.873	vw	2.875	2.876	w	2.876	2.885	ms	2.878	2.873	w
233	—	—	—	—	—	—	2.686	2.687	w	2.687	2.687	vvw	2.691	2.704	w
242	2.612	2.627	ms	2.617	2.624	ms	2.622	2.632	s	2.627	2.644	ms	2.632	2.642	s
243	2.351	2.368	vw	—	—	—	2.358	2.362	vw	2.360	2.364	vvw	2.364	2.370	vvw
035	2.108	2.116	vvw	2.108	2.117	vvw	2.108	2.120	w	2.108	2.125	vw	—	—	—
260	2.048	2.048	vw	—	—	—	—	—	—	2.064	2.058	vvw	—	—	—
353	1.945	1.956	vvw	1.949	1.950	w	1.953	1.958	ms	1.955	1.963	vw	1.960	1.960	ms
026	1.922	1.926	vvw	1.920	1.923	w	1.918	1.929	ms	1.916	1.933	vw	1.914	1.924	vw
163	1.882	1.879	vvw	1.887	1.878	vw	1.890	1.885	vw	1.893	1.891	vvw	1.897	1.879	vw
226	1.843	1.845	vvw	1.842	1.843	vvw	1.840	1.852	vw	—	—	—	1.840	1.843	vvw
270	1.778	1.775	vvw	1.784	1.783	vvw	—	—	—	1.793	1.791	vvw	—	—	—
236	1.755	1.749	vvw	1.755	1.750	vvw	1.754	1.757	vvw	1.754	1.765	vvw	—	—	—
046	1.709	1.716	vvw	1.709	1.702	vvw	—	—	—	1.708	1.710	vvw	1.707	1.703	vvw
173, 553	1.667	1.670	vvw	1.671	1.672	vw	1.674	1.674	vw	1.677	1.675	w	1.682	1.673	vw
246	1.652	1.648	vvw	1.653	1.647	vw	1.653	1.656	w	1.654	1.654	vvw	1.652	1.653	w
446	—	—	—	1.512	1.511	vvw	1.513	1.518	vvw	—	—	—	1.515	1.518	vvw
366	—	—	—	1.394	1.399	vvw	1.396	1.404	vvw	1.396	1.400	vvw	1.398	1.402	vvw
076	1.366	1.366	vvw	1.366	1.364	vvw	1.366	1.368	vvw	—	—	—	—	—	—
466	1.341	1.343	vvw	1.342	1.343	vvw	1.343	1.347	vw	1.344	1.349	vvw	1.345	1.344	vw
029	—	—	—	1.311	1.302	vvw	—	—	—	—	—	—	1.307	1.304	vvw
159	—	—	—	1.186	1.184	vvw	1.185	1.186	vvw	—	—	—	1.184	1.183	vvw
269	1.122	1.123	vvw	1.122	1.123	vvw	—	—	—	—	—	—	1.121	1.125	vvw
369	—	—	—	1.102	1.097	vvw	1.102	1.100	vw	—	—	—	—	—	—
379	1.054	1.049	vvw	1.054	1.052	vw	—	—	—	—	—	—	1.054	1.060	vvw

s = strong; ms = medium strong; w = weak; vw = very weak; vvw = very very weak.

TABLE III Observed and calculated lattice spacings of γ_2 non-equilibrium phase in aluminium-50 at.% germanium alloy.

Range of composition: $Al_{60}Ge_{40}$–$Al_{25}Ge_{75}$
Structure: Tetragonal
Lattice parameter: $a = 14.98$ Å $\simeq \sqrt{13}a_\alpha$
$c = 16.03$ Å $\simeq 4a_\alpha$
$c/a = 1.070 = 4/\sqrt{13}$

hkl	d_{cal}(Å)	d_{obs}(Å)	I_{obs}
222	4.429	4.257	vw
004	4.008		
040	3.745	3.703	vvw
024	3.538	3.541	w
042	3.401	3.401	vw
240	3.352	3.314	s
242	3.099	3.083	vvw
115	3.069		
333	2.954	2.997	w
151	2.899	2.861	ms
440	2.650	2.650	s
260	2.370	2.350	vw
353	2.321	2.317	vw
117	2.239	2.245	w
064	2.124	2.128	vvw
560	2.079	2.074	vw
008	2.004	2.010	vvw
371	1.959	1.957	vw
028	1.936	1.931	vw
080	1.873	1.882	vw
228	1.875		
464	1.850	1.850	vw
282	1.777	1.777	vvw
266	1.776		
571	1.737	1.747	vw
480	1.676	1.673	vvw
284	1.659	1.655	vvw
664	1.620	1.623	ms
484	1,550	1.552	vvw
680; 0, 10, 0	1.498	1.491	ms
359	1.465	1.461	w
773	1.461		
4, 10, 0	1.391	1.388	vvw
088	1.370	1.370	vvw
288	1.348	1.344	vvw
880	1.325	1.325	vw
668	1.327		
46, 10	1.271	1.275	vvw
884	1.261	1.258	vvw
04, 12	1.259		
688; 0, 10, 8	1.205	1.203	vvw
44, 12	1.193	1.191	vw
0, 12, 4	1.196		
15, 13	1.137	1.137	vvw
46, 12	1.125	1.123	vvw
888	1.108	1.113	vvw
6, 10, 8	1.083	1.082	vvw
28, 12	1.077	1.073	vvw
4, 10, 10	1.052	1.050	vvw
77, 11	1.051		
33, 15	0.987	0.985	w
28, 14	0.969	0.967	vvw
26, 16	0.923	0.918	vvw
0, 12, 12	0.914		
08, 16	0.884	0.880	vvw
28, 16	0.878		
66, 16	0.872	0.873	vvw

s = strong; ms = medium strong; w = weak; vw = very weak; vvw = very very weak

photographs of the same sample at regular intervals and estimating the proportion of the different phases. Only X-ray powder patterns taken after more than 10000 h of ageing at room temperature brought out detectable weakening of the reflections due to the non-equilibrium phase(s), along with an increase in intensity of the reflections due to the equilibrium phases. In fact, after 14 months of ageing γ_2 was found to be still retained in large proportion as evidenced by X-ray line intensities. But, in the case of γ_1 subjected to the same treatment, it was found to decompose, strengthening the X-ray line intensities of the equilibrium solid solutions. However, in case of experiments wherein the melt was dropped into water, the stability of the new phases seems to be quite low. In an Al-45 at. % Ge alloy rapidly solidified this way, the decomposition of γ_2 was quite appreciable even after ageing for one month at room temperature.

3.3. Constitution and Cooling Rate

Table IV gives the constitution at room temperature of Al—Ge alloys subjected to liquisol quenching. In spite of unavoidable fluctuations in the cooling rate, the proportion between the two main phases from among the four possible ones, namely fcc α (solid solution of Ge in Al), dc β (solid solution of Al in Ge), tetragonal γ_1 (first new non-equilibrium Al—Ge phase) and tetragonal γ_2 (second new non-equilibrium Al—Ge phase), appears to be reproducible within experimental error, as evaluated from the intensities of X-ray reflections from the coexisting phases. The distribution of phases in alloys quenched from the melt by dropping onto a copper substrate is not given in the above table for reasons mentioned earlier (section 2.2).

A non-equilibrium constitution diagram, fig. 4, is proposed for the Al—Ge system embodying all the results obtained so far. This is very similar to the diagrams proposed by Anantharaman *et al* for the Au—Ge [5] and Ag—Si and Au—Si [25] systems.

The non-equilibrium constitutional diagram (fig. 4) was constructed on the basis of visual estimation of the intensities of X-ray reflections from the various phases present at room temperature (table IV). As can be appreciated, it is unavoidable in such experiments that the X-ray sample contains flakes from different regions of the foils which had solidified at different cooling rates. Thus, the presence of more than two phases in some samples is not surpris-

TABLE IV Estimated distribution of phases in aluminium-germanium alloys rapidly solidified from the melt.

At. % Ge	Melt shot onto a copper substrate				Melt shot into water				Melt dropped into water			
	α-fcc	γ_1-tetragonal	γ_2-tetragonal	β-dc	α-fcc	γ_1-tetragonal	γ_2-tetragonal	β-dc	α-fcc	γ_1-tetragonal	γ_2-tetragonal	β-dc
5	vs	—	—	—	vs	—	—	vvw	vs	—	—	vvw
10	vs	—	—	vvw	vs	—	—	vw	vs	—	—	vw
15	s	w	—	vw	s	w	—	vw	s	—	—	w
20	ms	w	—	vvw	ms	ms	—	vvw	s	w	—	vw
25	m	ms	—	tr	w	s	—	—	ms	ms	—	vw
30	w	vs	—	—	vw	vs	—	—	m	ms	w	w
33.3	vw	vs	—	—	w	w	s	—	w	vw	s	w
40	vvw	s	ms	—	w	—	ms	w	vvw	—	w	s
45	—	—	s	vw	vw	—	w	s	w	—	w	s
50	—	—	vs	vw	vw	—	w	s	w	—	vw	s
60	—	—	s	vw	vw	—	vw	vs	vw	—	vvw	s
70	—	—	ms	w	vw	—	vvw	vs	vw	—	vvw	vs
75	—	—	w	w	vvw	—	vvw	vs	vw	—	vvw	vs
80	vvw	—	tr	vs	vvw	—	tr	vs	vw	—	tr	vs
90	vw	—	—	vs	vvw	—	—	vs	vw	—	—	vs

vs = very strong; s = strong; ms = medium strong; m = medium; w = weak; vw = very weak; vvw = very very weak; tr = trace.

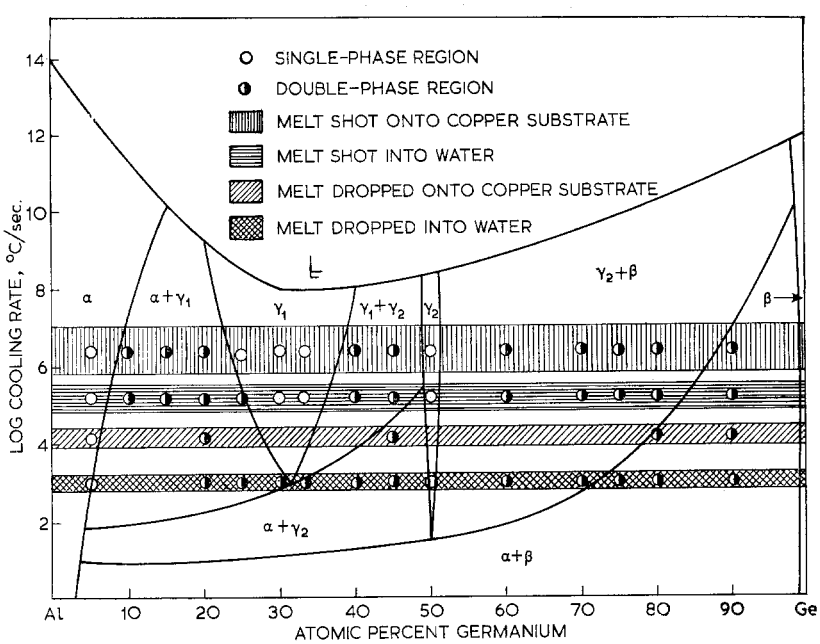

Figure 4 Relation between cooling rate and constitution at room temperature in Al—Ge system.

ing, the third phase generally arising from lower cooling rates and causing weak X-ray reflections. Such third phases have been ignored in marking the points and drawing the phase boundaries in fig. 4.

The retention of the liquid structure has been taken to be the easiest, i.e. possible at the lowest cooling rate, at the equilibrium eutectic composition, since the probability of retaining the liquid structure has been shown to be the highest at or around eutectic composition in various systems [26]. Further, liquid Ge has been shown to be capable of retention at lower cooling rates than in case of liquid Al. This is based on the observa-

tion that Ge can be solidified comparatively easily in an amorphous state either by vapour deposition or electrodeposition techniques [27].

The maximum solid solubility of 7.2 at. % Ge in Al was observed only in the liquisol-quenching "gun" technique. Therefore, a sloping "solvus" line has been drawn on the Al-rich side of the diagram. On the Ge-rich side, no increase in solid solubility of Al in Ge could be observed and hence the "solvus" line is shown steep. Since the solid solubility may possibly be enhanced at still higher cooling rates than employed in the present work, a small slope has been shown at very high cooling rates.

The phase boundaries for γ_1 and γ_2 phases have been drawn on the basis of their occurrence in alloys subjected to different cooling rates. At their critical cooling rates for the alloys containing 33.3 and 50.0 at. % Ge, the non-equilibrium constitutional diagram resembles a "eutectoid" reaction in a conventional phase diagram.

4. Discussion

4.1. Solid Solubility Limits

The present study has shown that the solid solubility of Ge in Al can be increased by subjecting the alloys to rapid solidification techniques. Although, the extension of solid solubility limit of Ge in Al by a similar technique was reported earlier [7], the exact amount of extension was not mentioned. However, from our work on dilute alloys and from a measurement of the lattice parameters in duplex alloys, it could be concluded that a maximum of 7.2 at. % Ge can be dissolved in Al in the solid state.

Although electronegativity and size factor are favourable for formation of extensive solid solutions in the Al—Ge system, the differences in valency and crystal structure preclude extensive solid solubility on either side. Extension of solid solubility on liquisol-quenching has been observed in some Al-base alloys namely, Al—Ag [28], Al—Mg [29], Al—Ti [30], Al—Si [31] and Al—Au [32]. But in no case has the extension been beyond the eutectic composition. This is understandable because nucleation of the second phase becomes easier in hypereutectic alloys and effectively prevents further increase in solubility beyond the eutectic composition. In the above-mentioned cases, the ratios of the limits of extended solid solubility to the equilibrium solid solubility work out to 1.6, 2.0, 2.6, 7.0 and 8.5 respectively. In case of Al—Ge alloys the ratio is only 2.6, which is far lower than the ratio of 7.0 in the homologous system Al—Si, where a maximum of 11.3 at. % Si could be dissolved in Al by liquisol quenching. These two systems are, however, not strictly comparable, since no non-equilibrium intermediate phase seems to form in Al—Si system even at very high cooling rates [31], whereas the intermediate phase γ_2 forms even at comparatively lower cooling rates in the Al—Ge system. However, from an observation of the intensity distribution of various phases, it has been concluded that the α solid solution forms in a more supersaturated state than has been observed and then it decomposes, rather fast, to equilibrium α and β solid solutions.

In accordance with the behaviour of IVB group elements with metals like Au and Ag, an increase in solid solubility of Al in Ge on quenching from the melt is not to be expected. Although the X-ray diffraction patterns of quenched alloys at very low concentrations of Al contained reflections due only to β, there was no lattice parameter evidence for any change in the solid solubility limit. Probably, higher cooling rates than those employed in the present investigation might lead to some enhancement of solid solubility.

4.2. The γ_1 Phase

The formation of an intermediate phase in an Al-30 at. % Ge alloy has been briefly reported by us [18] earlier. This phase, designated as γ_1, is now found to occur over a range of composition, namely, between 15 and 40 at. % Ge. This phase is always present along with α solid solution and is rarely obtained as a completely homogeneous single phase. The regular and constant variation in the interplanar spacings of the extra lines occurring in this composition range strongly suggests that the lattice parameters of this phase do vary as a function of the germanium content of the alloy. Further, the mean atomic volume calculated for this phase at different compositions, assuming that the phase is as close-packed as the α solid solution and on the basis of 120 atoms per unit cell, falls on a smooth straight line drawn between the mean atomic volumes of pure Al and pure Ge [33], as shown in fig. 5. From the intensities of the X-ray reflections at different compositions, it is clear that this phase forms most easily between 30 and 33.3 at. % Ge. Hence, we might assign a formula Al_2Ge for this non-equilibrium phase, although for reasons not so obvious it displays a wide range of composition.

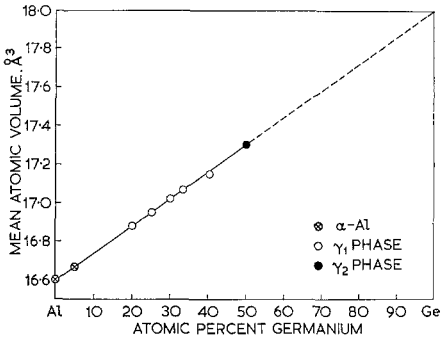

Figure 5 Variation of mean atomic volume of liquisol-quenched Al—Ge alloys with Ge content.

The difficulty in producing a strictly homogeneous γ_1 can be accounted for by postulating the complete crystallisation of the melt into homogeneous γ_1 and its subsequent partial decomposition while cooling down to its normal decomposition temperature. The decomposition in the solid state is facilitated by the slower cooling rate due to the evolution of latent heat of fusion. However, only a small fraction of γ_1 seems to decompose to α and β solid solutions and since the amount of β phase is small, only traces of it are observed in the X-ray powder patterns.

4.3. The γ_2 Phase

At higher germanium concentrations also, a large number of extra reflections appear in addition to those due to the equilibrium β solid solution. These reflections continue to appear from 40 to 80 at. % Ge. As can be seen from table III, all the (*hkl*) values for these reflections are all odd or all even and thus characteristic of a face-centred lattice. This seems to be one of the characteristic differences between the γ_1 and γ_2 structures. Comparing tables II and III, one is bound to come across some common interplanar spacings. But, judging from the number of reflections, the variation in intensity and the appreciable difference in many of the interplanar spacings, one has to index these extra lines on the basis of another structure. Further, all the reflections in this range of composition could not satisfactorily be indexed on the basis of only the γ_1 phase. Moreover, assuming the same efficiency of packing as in α solid solution and 208 atoms per unit cell, the mean atomic volume calculated for this alloy composition falls on the same straight line as before (fig. 5). Yet another difference between γ_1 and γ_2 phases is that, whereas the former exhibits a wide range of occurrence, the latter does not have any lattice parameter variation. However, neither occurs homogeneously and the stability of the two phases does not seem to be very much different. Lower cooling rates or higher germanium contents seem to favour, however, the formation of γ_2 in preference to γ_1. From the intensity of the various reflections observed over a wide range of composition, the γ_2 phase might be considered to form most easily around 50 at. % Ge and hence assigned the formula AlGe.

4.4. Crystal Chemistry of the New Phases

The relationships between the *a* parameters of the γ_1 and γ_2 structures and the lattice parameter of α solid solution are brought out with reference to the (001) plane of α fcc phase in fig. 6. The

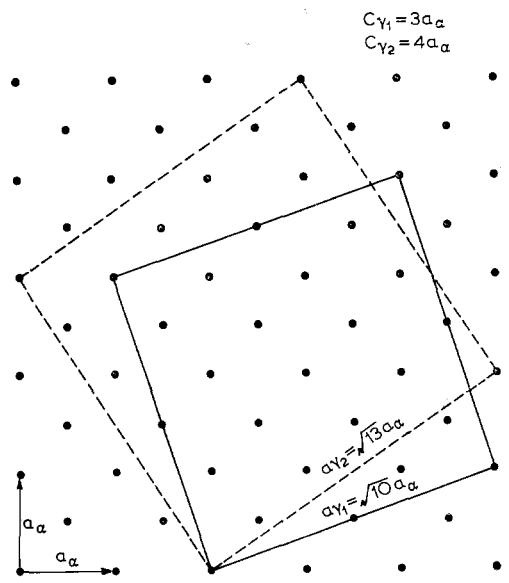

Figure 6 Representation of the lattice vectors corresponding to the two new Al—Ge tetragonal phases on the (001) plane of α solid solution.

face-diagonal of the rectangle formed by three unit cells in the x-direction and one in the y-direction may be considered as the *a* parameter of γ_1 while the face diagonal of the rectangle formed by three unit cells in the x-direction and two in the y-direction may be looked upon as the *a* parameter of γ_2. The *c* parameters for γ_1 and γ_2 are approximately three and four times, respectively, of the lattice parameter of α solid solution.

The occurrence of these two tetragonal structures can possibly be understood as follows.

For the γ_1 structure, the a parameter which is approximately equal to $\sqrt{10}a_\alpha$ is continuously increasing from 12.91 Å at 15 at. % Ge to 13.11 Å at 40 at. % Ge. In the same composition range, $\sqrt{10}a_\alpha$, i.e. $\sqrt{10}$ times the lattice parameter of the hypothetical α solid solution, increases from 12.88 Å at 15 at. % Ge to 13.01 Å at 40 at. % Ge. As can be clearly seen from the a parameter of the γ_1 phase, the actual increase is more than expected from the increase in a_α. This greater increase is counterbalanced, for the retention of atomic volume, by a decrease in the c parameter of the γ_1 phase. If it is assumed that both γ_1 and γ_2 are as close-packed as the α-solid solution, then one criterion for choosing the lattice parameters of the new phases is that they must be representable by a vector joining two atoms in fig. 6. Although the a parameter for γ_1 is increasing, it cannot go on increasing continuously without delecting the next possible minimum vector, which is obviously $\sqrt{13}a_\alpha$ (= 14.90 Å) and this is approximately the same as the a parameter of γ_2 (14.98 Å).

The frequent occurrence of 3 or its multiples in table II and IV or its multiples in table III for values of l in the Miller indices (hkl) of reflections lend some support for the suggestion that $c_{\gamma_1} \simeq 3a_\alpha$ and $c_{\gamma_2} \simeq 4a_\alpha$. It was observed that γ_1 is obtained at lower germanium contents and γ_2 at higher germanium contents.

At present, it seems rather difficult to explain the observed difference in X-ray diffraction behaviour between the γ_1 and γ_2 structures. One possibility is that since the a parameter of γ_1 is varying as a function of germanium content, the positions of atoms might be somewhat different from what they are in the α solid solution. This will give rise to incidence of X-ray reflections from practically all crystallographic planes. On the other hand, in the case of γ_2, the displacement of atoms might be marginal and hence one might expect reflections characteristic of a face-centred lattice. Further, the production of γ_2 at lower cooling rates and γ_1 at higher cooling rates in the same alloy suggests that the distortion of the lattice is greater for the formation of γ_1. The difficulty in producing a suitable and completely homogeneous sample for a thorough structure analysis precludes the possibility of locating the atom positions exactly.

4.5. Influence of Cooling Rate

The cooling rates in the present investigation have been estimated on the basis of secondary DAS measurement. They are about 10^6 to 10^7°C/sec when the alloy was shot onto a copper substrate and about 10^4°C/sec when the melt was dropped onto a copper substrate without a shock wave. As has already been indicated, these estimates are likely to be on the higher side in the former case and on the lower side in the latter case. Hence the cooling rate in experiments where the melt was shot into water was assumed to be intermediate between the two, i.e. about 10^5°C/sec. When the melt was just dropped into water it was roughly estimated to be around 10^3°C/sec. The constitution, at room temperature, of the Al—Ge alloys at different cooling rates is depicted in fig. 4. At all the rates of cooling employed in this work non-equilibrium structures are formed. Still lower cooling rates of the order of 10^2°C/sec were tried by simple solid state quenching of the alloys, but no non-equilibrium phase resulted. Hence, we have strong reason to believe that the critical cooling rate for the formation of the new phases in Al—Ge system lies somewhere between 10^2 and 10^3°C/sec. The proposed non-equilibrium constitution diagram brings out these salient features rather well. This diagram not only seems to explain all the observed phenomena, but also may be used to predict the constitution for any composition for a chosen cooling rate.

5. Conclusions

Liquisol-quenching of Al—Ge alloys has revealed the existence of two non-equilibrium intermediate phases γ_1 and γ_2 in the composition ranges 15 to 40 and 40 to 80 at. % Ge, respectively. These phases were found to be tetragonal with $a_{\gamma_1} \simeq \sqrt{10}a_\alpha$, $c_{\gamma_1} \simeq 3a_\alpha$ and $a_{\gamma_2} \simeq \sqrt{13}a_\alpha$, $c_{\gamma_2} \simeq 4a_\alpha$. Quenching of the alloys at lower cooling rates was found to be congenial for the formation of γ_2 at lower germanium concentrations, whereas at higher cooling rates γ_1 was found to form. A new non-equilibrium constitution diagram is proposed to explain the observed phenomena.

Acknowledgements

The authors are grateful to their colleague Dr P. Ramachandrarao for many helpful discussions and Mr P. K. Garg of the Department of Physics, Banaras Hindu University, for help in electron-microscopic work.

References

1. POL DUWEZ and R. H. WILLENS, *Trans. AIME* **227** (1963) 362.

2. P. PREDECKI, A. W. MULLENDORE, and N. J. GRANT, *ibid* **233** (1965) 1581.
3. R. C. RUHL, *Mat. Sci. Engg.* **1** (1967) 313.
4. POL DUWEZ, R. H. WILLENS, and W. KLEMENT, JR., *J. Appl. Phys.* **31** (1960) 1137.
5. T. R. ANANTHARAMAN, H. L. LUO, and W. KLEMENT, JR., *Trans. AIME* **233** (1965) 2014.
6. *Idem, Nature* **210** (1966) 1040.
7. P. PREDECKI, B. C. GIESSEN, and N. J. GRANT, *Trans. AIME* **233** (1965) 1438.
8. B. C. GIESSEN, *Z. Metalk.* **59** (1968) 805.
9. R. H. KANE, B. C. GIESSEN, and N. J. GRANT, *Acta Met.* **14** (1966) 605.
10. R. C. RUHL, B. C. GIESSEN, M. COHEN, and N. J. GRANT, *ibid* **15** (1967) 1693.
11. POL DUWEZ, *Trans. Amer. Soc. Metals* **60** (1967) 607.
12. *Idem, Prog. Solid State Chem.* **3** (1966) 377.
13. B. C. GIESSEN, "Proceedings of the 12th Army Materials Research Conference" (Syracuse University Press, Syracuse, N.Y., 1966) p. 273.
14. P. RAMACHANDRARAO, "Structural Studies in Metals and Alloys Rapidly Cooled from the Melt", Ph.D. Thesis, Banaras Hindu University, India (1968).
15. P. FURRER, T. R. ANANTHARAMAN, and H. WARLIMONT, *Phil. Mag.* **21** (1970) 873.
16. A. TONEJC and A. BONEFAČIĆ, *J. Appl. Phys.* **40** (1969) 419.
17. R. P. ELLIOTT, "Constitution of Binary Alloys: First Supplement" (McGraw-Hill Book Co., New York, 1965) p. 38.
18. C. SURYANARAYANA and T. R. ANANTHARAMAN, *Current Sci.* **37** (1968) 631.
19. *Idem, ibid* **39** (1970) 123.
20. P. RAMACHANDRARAO, P. RAMA RAO, and T. R. ANANTHARAMAN, *Z. Metalk.* **61** (1970) 471.
21. K. LÖHBERG and H. MÜLLER, *ibid* **60** (1969) 231.
22. H. MATYJA, B. C. GIESSEN, and N. J. GRANT, *J. Inst. Metals* **96** (1968) 30.
23. S. A. LEVY, R. E. HUGHES, and A. I. KEMPPINEN, *AFS Cast Metals Res. J.* **5** (1969) 93.
24. H. J. AXON and W. HUME-ROTHERY, *Proc. Roy. Soc.* **A193** (1948) 1.
25. H. L. LUO, W. KLEMENT, JR., and T. R. ANANTHARAMAN, *Trans. Ind. Inst. Metals* **18** (1965) 214.
26. W. HUME-ROTHERY and E. ANDERSON, *Phil. Mag.* **5** (1960) 383.
27. H. S. CHEN and D. TURNBULL, *J. Appl. Phys.* **40** (1969) 4214.
28. J. DIXMIER and A. GUINIER, *Mem. Sci. Rev. Met.* **64** (1967) 53.
29. H. L. LUO, C. C. CHAO, and POL DUWEZ, *Trans. AIME* **230** (1963) 1488.
30. A. TONEJC and A. BONEFAČIĆ, *Scripta Met.* **3** (1969) 145.
31. M. ITAGAKI, B. C. GIESSEN, and N. J. GRANT, *Trans. Amer. Soc. Metals* **61** (1968) 330.
32. T. TODA and R. MADDIN, *Trans. AIME* **245** (1969) 1045.
33. P. S. RUDMAN, *ibid* **233** (1965) 864.

Received 12 May and accepted 27 August 1970.